Vibron Quasibound State in the Noncentrosymmetric Tetragonal Heavy-Fermion Compound $CeCuAl_3$

D. T. Adroja,[1,*] A. del Moral,[2] C. de la Fuente,[2] A. Fraile,[1] E. A. Goremychkin,[1,‡] J. W. Taylor,[1] A. D. Hillier,[1] and F. Fernandez-Alonso[1,†]

[1]*ISIS Facility, Rutherford Appleton Laboratory, Chilton, Didcot, Oxon OX11 0QX, United Kingdom*
[2]*Laboratorio de Magnetismo, Depto Física Materia Condensada, Universidad de Zaragoza & ICMA, Spain*

(Received 11 January 2012; published 23 May 2012)

We have investigated the noncentrosymmetric tetragonal heavy-fermion antiferromagnetic compound $CeCuAl_3$ ($T_N = 2.5$ K) using inelastic neutron scattering (INS). Our INS results unequivocally reveal the presence of three magnetic excitations centered at 1.3, 9.8, and 20.5 meV. These spectral features cannot be explained within the framework of crystal-electric-field models and recourse to Kramers' theorem for a $4f^1$ Ce^{3+} ion. To overcome these interpretational difficulties, we have generalized the vibron model of Thalmeier and Fulde for cubic $CeAl_2$ to tetragonal point-group symmetry with the theoretically calculated vibron form-factor. This extension provides a satisfactory explanation for the position and intensity of the three observed magnetic excitations in $CeCuAl_3$, as well as their dependence on momentum transfer and temperature. On the basis of our analysis, we attribute the observed series of magnetic excitations to the existence of a vibron quasibound state.

DOI: 10.1103/PhysRevLett.108.216402 PACS numbers: 71.27.+a, 71.70.Ch, 75.30.Mb, 78.70.Nx

Strongly correlated electron systems exhibiting spin, charge, and lattice degrees of freedom can sustain elementary excitations arising from localized, single-ion crystal electric fields (CEFs) as well as dispersive vibrational modes (phonons). Although both types of excitations have very similar energy scales, they are in general considered to be decoupled from each other [1]. Consequently, these two phenomena, i.e., CEF energy levels and phonon dispersion relations, are investigated independently. It is well known, however, that electron-phonon (e-p) coupling gives rise to novel and subtle phenomena. Such is the case of BCS-type superconductivity (SC) where e-p coupling occurs because phonons distort the local lattice structure as they propagate, and conduction electrons respond to the resulting band distortion. In this context, it is still an open question what happens when CEF-phonon coupling (c-ph, i.e., the coupling between local electronic spin or orbital degrees of freedom and phonons) is switched on in strongly correlated rare-earth-based materials. To date, signatures of strong c-ph coupling have only been observed in a handful of strongly correlated compounds, namely, $CeAl_2$ [2–4], $YbPO_4$ [5], $CePd_2Al_2$ [6], $CeCu_2$ [3], $(PrY)Ni_2$ and $(PrLa)Ni_2$ [7], and the insulator PrO_2 [8]. Among these, the cubic compound $CeAl_2$ is a well-known example of this phenomenon and has been investigated extensively using various experimental techniques [2,3]. To explain the excitation spectrum of $CeAl_2$, a c-ph coupling model was proposed for a cubic system by Thalmeier and Fulde some time ago [4]. This model features strong magnetoelastic (MEL) coupling between orbital and lattice degrees of freedom resulting in well-defined changes to macroscopic observables as well as a new type of (hybrid) magnetic-phonon mode [2–8].

In this Letter, we report unambiguous experimental and theoretical evidence of strong c-ph coupling in the tetragonal heavy-fermion (HF) antiferromagnetic (AFM) compound $CeCuAl_3$ [8–10]. $CeCuAl_3$ crystallizes in a noncentrosymmetric (NCS) tetragonal $BaNiSn_3$-type structure, space group I4 mm, see Fig. 1(a) [9], where magnetic Ce^{3+} ions are arranged in a body-centered tetragonal sublattice. $BaNiSn_3$-type HF compounds have recently attracted much attention concerning SC in a NCS lattice.

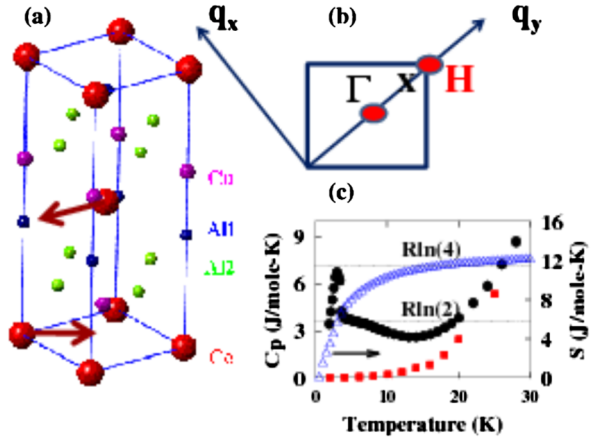

FIG. 1 (color online). (a) Tetragonal unit cell for $CeCuAl_3$. The arrows represent the active longitudinal optic (L-optic) phonon modes at the H-point of the Brillouin zone (BZ) with $^1H_3$ symmetry. The displacement vector $\mathbf{u}$ is the same for all other Ce^{3+} ions in the unit cell. (b) The square BZ for the basal plane, showing the location of the H point. (c) Heat capacity (left y axis) of $RCuAl_3$ (R = Ce, black circles and R = La, red squares) and magnetic entropy (right y axis) versus temperature.

For example, $CeRhSi_3$ and $CeIrSi_3$ exhibit pressure-induced SC near the quantum critical point [10,11]. It has been proposed that the underlying NCS symmetry leads to the violation of parity conservation of the Cooper-pair state and that an admixture of singlet and triplet spin states serves to stabilize it [10,11]. Thus, the investigation of $BaNiSn_3$-type HF metals in connection with their strong electron-electron and electron-phonon interactions constitutes a topical and largely unexplored area. The present work focuses on the properties of $CeCuAl_3$. Below 15 K, its heat capacity (C/T) increases with decreasing temperature and exhibits a λ-type anomaly at 2.5 K due to the ordering of Ce-centered magnetic moments [12,13]. The associated Sommerfeld coefficient and Kondo temperature are $\gamma_{\mathrm{el}} = 140\ \mathrm{mJ/mole\,K^2}$ and $T_{\mathrm{K}} = 8$ K, respectively [12]. The temperature dependence of the single-crystal magnetic susceptibility reveals a ground state (GS) $|\pm 1/2\rangle$, resulting in a CEF splitting between ground and first excited states of 10 K, followed by a second CEF doublet at 180 K [13]. A type-I AFM structure with magnetic moment $0.2\mu_{\mathrm{B}}$/Ce parallel to the c axis has been reported in single-crystal neutron diffraction experiments [14].

Polycrystalline samples (mass ~30 g) of $CeCuAl_3$ and its phonon reference $LaCuAl_3$ were prepared by the standard arc-melting method starting with a stoichiometric mixture of high-purity elements (Ce, La: 99.9%; Cu: 99.99%; Al: 99.999%). The as-cast samples were annealed for a week at 900 °C under vacuum to improve single-phase formation. Phase purity was checked at 300 K on the GEM diffractometer at the ISIS Facility, Rutherford Appleton Laboratory, U.K. Analysis of these diffraction data using the GSAS program confirmed the single-phase, $BaNiSn_3$-type tetragonal structure of the samples, in agreement with previous reports [9]. Heat capacity measurements were performed by the relaxation method using a PPMS system (Quantum-Design). The INS measurements were carried out between 4.7 and 150 K on the time-of-flight spectrometer MARI, also at the ISIS Facility. Measurements were performed at three incident neutron energies, namely, $E_i = 6$, 8, and 40 meV.

The heat capacity data reported in Fig. 1(c) exhibit a broad peak near 6 K and a λ-type transition at 2.5 K. The former is due to a Schottky anomaly arising from the low-energy CEF doublet (at 10 K), as inferred from a susceptibility analysis [13], whereas the latter arises from the AFM ordering of the Ce moments. The temperature dependence of the magnetic entropy has been estimated by subtracting the phonon contribution using $LaCuAl_3$ data and shows that the entropy is $\sim R\ln(2)$ at 2.6 K and $\sim R\ln(4)$ at 20 K. This result is also in agreement with the predicted CEF energy-level structure derived from the susceptibility measurements [13].

Figures 2(a) and 2(b) show the INS spectra for $RCuAl_3$ (R = Ce, La) at a temperature $T = 4.7$ K at incident energy $E_i = 40$ meV and (d)–(e) at 8 meV. It is clear from these data that $CeCuAl_3$ exhibits three magnetic excitations near 1.3, 9.8, and 20.5 meV at low momentum transfers Q, while there is no discernibly strong phonon scattering in $LaCuAl_3$ at these energies. These stark differences in spectral response are evident in the low-Q (0–4 $\mathrm{Å}^{-1}$) and high-Q (5–10 $\mathrm{Å}^{-1}$) 1D cuts shown in Fig. 3. At 4.7 and 150 K, the phonon contributions at high-Q are similar in both compounds after taking into account differences in neutron scattering cross sections. At

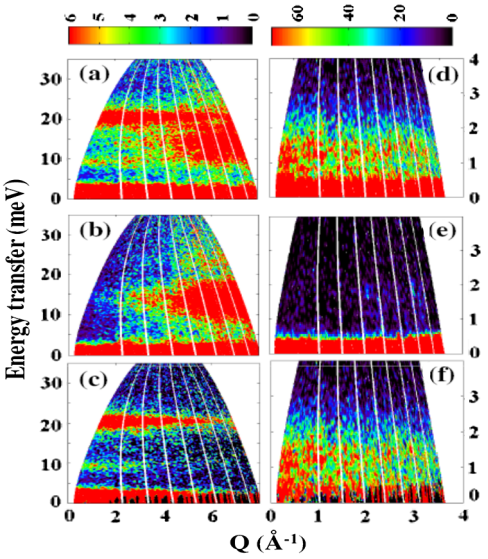

FIG. 2 (color online). Contour plots of the INS data as a function of energy transfer (E) and momentum transfer (Q): (a) $CeCuAl_3$ and (b) $LaCuAl_3$ at 4.7 K with an incident energy $E_i = 40$ meV; (d) $CeCuAl_3$ and (e) $LaCuAl_3$ at 4.7 K with incident energy $E_i = 8$ meV. Magnetic scattering in $CeCuAl_3$ at 4.7 K has been estimated by subtracting the data of $LaCuAl_3$ as show in panels (c) and (f) for $E_i = 40$ meV and 8 meV, respectively.

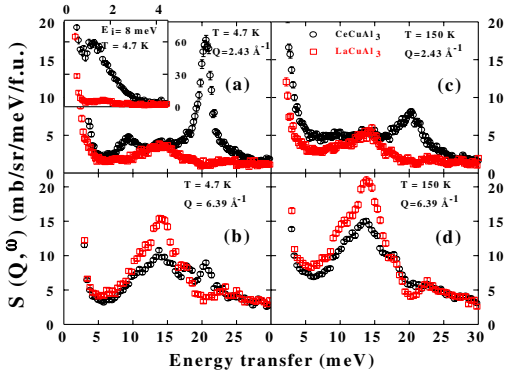

FIG. 3 (color online). Q-integrated 1D cuts of the total scattering from $CeCuAl_3$ (black circles) and $LaCuAl_3$ (red squares) at low $Q = 0$ to 4(2.43) $\mathrm{Å}^{-1}$ (a, c) and at high $Q = 5$ to 10(6.39) $\mathrm{Å}^{-1}$ (b, d) at 4.7 and 150 K (right side). The inset shows the data from $CeCuAl_3$ and $LaCuAl_3$ with $E_i = 8$ meV ($Q = 0$ to 3.6(2.0) $\mathrm{Å}^{-1}$) at 4.7 K.

low-Q's, the magnetic scattering is strong in $CeCuAl_3$, with a small phonon contribution. An approximate magnetic-scattering law has been deduced by subtracting the observed scattering for $LaCuAl_3$ from that of $CeCuAl_3$, i.e., $S_M(Q,\omega) = S(Q,\omega;\mathrm{CeCuAl_3}) - \alpha S(Q,\omega;\mathrm{LaCuAl_3})$, where $\alpha = 0.693$ is the ratio of total-scattering cross sections for $CeCuAl_3$ and $LaCuAl_3$. The results of this subtraction procedure are shown in Figs. 2(c) and 2(f). As a further check on the physical origin of these spectral features, Fig. 4 shows their energy-integrated intensities as a function of Q. The intensity of all three excitations decreases with increasing Q, following the square of the magnetic form factor, $F^2(Q)$, for a Ce^{3+} ion.

As $CeCuAl_3$ contains Ce^{3+} ions in a $4f^1$ electronic configuration ($J = 5/2$), Kramers' theorem dictates that all CEF levels should be doubly degenerate. Therefore, the observed three CEF excitations from the ground state in $CeCuAl_3$ (above T_N) cannot be explained on the basis of a pure CEF model involving tetragonal point-group symmetry. In such a case, the associated CEF Hamiltonian is of the form $H_{\mathrm{CEF}} = B_2{}^0\mathrm{O}_2{}^0 + B_4{}^0\mathrm{O}_4{}^0 + B_4{}^4\mathrm{O}_4{}^4$, where $\mathrm{O}_n{}^m$ are Stevens operators [15] and $B_n{}^m$ are CEF parameters. We attempted to fit the INS data based on the pure CEF model and found a good fit for the observed spectral features at 1.3 meV and 20.5 meV, but the peak at 9.8 meV could not be accounted for. This result indicates that this peak cannot arise from pure CEF excitations, but from a new kind of excitation. This is a similar situation to that found in cubic $CeAl_2$, which reveals two CEF excitations, yet one expects only one originating from the ground state [2–4]. The case of $CeAl_2$ was explained by the c-ph coupling model of Thalmeier and Fulde [4]. In this phenomenological model, the two key ingredients to achieve a stronger coupling between CEF and phonon excitations are (1) the phonon frequency ($\hbar\omega_0$) should be close to the CEF level; and (2) the phonon and CEF eigenfunctions should have similar symmetry. In addition to these necessary ingredients, the strength of MEL coupling must be sizeable and we have no control on this. The high phonon density of states (PDOS) close to CEF levels favors MEL coupling. To explain the present results on $CeCuAl_3$, we have generalized the cubic c-ph (MEL) coupling model to tetragonal point-group symmetry (first used by Chapon *et al.* [6]) with the proper vibron form factor. The total Hamiltonian (H_{tot}) contains three terms of the form [4]:

$$H_{\mathrm{tot}} = H_{\mathrm{CEF}} + \hbar\omega_0(a_u^+ a_u + 1/2) - M^{\gamma,2}(a_u + a_u^+)O_u, \quad (1)$$

where the first term is the tetragonal CEF Hamiltonian mentioned above, the second term is the phonon Hamiltonian (H_{ph}), and the third term is the MEL (c-ph)-coupling term ($H_{c\text{-ph}}$). Here $\hbar\omega_0$ denotes the phonon energy, and $a_{\mathbf{u}}{}^+$ or $a_{\mathbf{u}}$ are phonon creation or annihilation operators. In this second-quantization picture, ion displacements are given by the operator $\hat{\mathrm{U}} = (a_{\mathbf{u}}{}^+ + a_{\mathbf{u}})$, where $\mathbf{u}$ is the phonon displacement [4,16]. $M^{\gamma,2}$ is a magnetoelastic parameter proportional to the coupling between CEF and phonon excitations. O_u is the CEF-phonon operator and its symmetry was determined using a double-valued (d.v.) representation for the direct products of the $\Gamma_\alpha \otimes \Gamma_H$ irreducible representations (IRs) where $\propto = 6, 7, 6'$ correspond to pure CEF doublets. With these considerations in mind, one can explore which regions of the Brillouin zone (BZ) should display strong CEF-phonon couplings. Such a region should have a high PDOS and, therefore, the associated phonon dispersion relation should have zero slope. Figure 1(b) shows the BZ associated with the basal plane where Ce^{3+} ions display square symmetry.

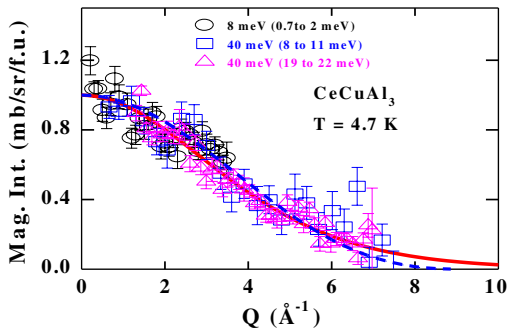

FIG. 4 (color online). Energy-integrated Q-dependent magnetic scattering from $CeCuAl_3$ at 4.7 K. The solid line (red) represents the square of the Ce^{3+} magnetic form factor and the dotted line (blue) represents the vibron structure factor (see text).

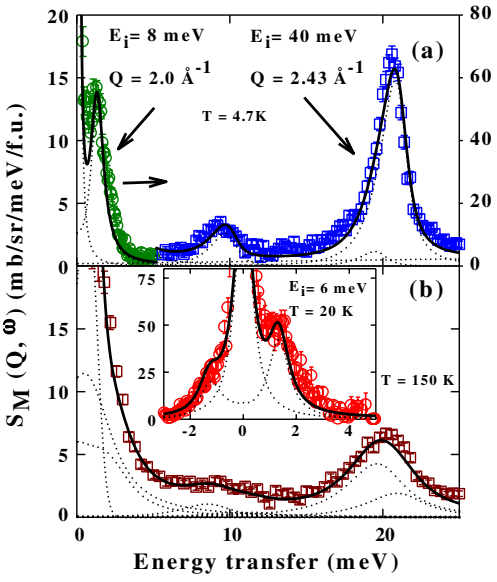

FIG. 5 (color online). Low-Q (2.43 $\mathrm{Å}^{-1}$) magnetic scattering in $CeCuAl_3$ at 4.7 K (a) and 150 K (b) at an incident energy $E_i = 40$ meV. The green circles in (a) correspond to $E_i = 8$ meV (right y axis). The inset in (b) shows the data with $E_i = 6$ meV at 20 K and $Q = 1.7$. $\mathrm{Å}^{-1}$. The thick solid lines represent the fit using the Hamiltonian given by Eq. (1). The dotted lines show the individual components to the fit (see text for details).

At the BZ H point, there are five phonon IRs, namely: one volume (α), one tetragonal (γ), two pseudo-trigonal (ε_1, ε_2) and one orthorhombic (δ or $^1H_3$) mode [16]. Of these five, symmetry arguments dictate that only the orthorhombic $^1H_3$ phonon mode couples to the CEF doublets. Since $^1H_3$ transforms as x^2-y^2, the CEF-phonon (or MEL) operator must be of the form $O_u = O_2^2 = {J_x}^2 - {J_y}^2 = 1/2({J_+}^2 + {J_-}^2)$ in the angular-momentum representation. Using this result, magnetic INS spectra were calculated via recourse to the following dipolar spectral function connecting two energy levels E_α and E_β:

$$S_{\alpha\beta}(Q,\omega) = \sum_{m,n}^{\alpha\beta} p_\alpha d_{\alpha\beta}^{nm} F_{\mathrm{vib}}^2(Q)\delta(E_\alpha - E_\beta - \hbar\omega), \quad (2)$$

where the oscillator strength is given by $d_{\alpha\beta}^{nm} = |\langle {}^2\Gamma_\alpha^n \boldsymbol{u}|J_\perp|{}^2\Gamma_\beta^m \boldsymbol{u}'\rangle|^2$. F_{vib}^2 is the vibron form-factor $F_{\mathrm{vib}}^2(Q) = C[\sin(Qd/2)/(Qd/2)]^2$ where $C \sim 0.95$ and $d = 0.7$ Å have been obtained from a fit of the Q-dependent intensities shown in Fig. 4. $|{}^2\Gamma_\alpha^n, \boldsymbol{u}\rangle$ correspond to the vibron eigenfunctions obtained from Eq. (1) where n is the CEF doublet index. p_α is the thermal occupation number of the vibronic multiplet and J is the component of the total angular momentum perpendicular to the scattering vector. $d_{\alpha\beta}^{nm}$ describes the magnetic dipole transition. The starting point of our analysis was to search for suitable CEF parameters that can result in a high-lying CEF peak in the vicinity of a correspondingly high PDOS close to 13.5 meV, as well as a low-energy peak near 1.3 meV. To explore the effects of MEL interactions, CEF parameters were kept fixed and INS spectra were simulated by varying $M^{\gamma,2}$ from 0 to 0.5 in 0.1 meV steps while keeping $\hbar\omega_0$ fixed at a value of 13.5 meV. When $M^{\gamma,2}$ was close to 0.2 meV, we observed the splitting of the 15 meV peak and such a splitting increased with increasing $M^{\gamma,2}$, yet no strong energy renormalization effects were found for the position of the low-energy feature at 1.3 meV. These simulations revealed that $M^{\gamma,2}$ lies between 0.4 and 0.5 meV. A final refinement of this protocol was carried out via a simultaneous fit of the INS data at 4.7 K for all three incident energies, namely, $E_i = 6$ meV (also 20 K data set), 8, and 40 meV (also 150 K data set). In the final fit (cf. Fig. 5), we allowed changes to the CEF parameters, $\hbar\omega_0$, and $M^{\gamma,2}$ yielding the following values in meV: ${B_2}^0 = 0.611(0.017)$, ${B_4}^0 = -0.015(0.001)$, $|{B_4}^4| = 0.317(0.004)$, $\hbar\omega_0 = 11.3(0.5)$, and $M^{\gamma,2} = 0.40(0.03)$ meV/Ce^{3+}. Please note that from the INS data one cannot determine the sign of ${B_4}^4$. These parameters give rise to a pure CEF G.S. with wave function $|\pm 1/2\rangle$ in agreement with previous susceptibility analyses [14]. Moreover, the estimated ordered-state Ce moment is $\langle\mu_x\rangle = 1.4\mu_B$ and $\langle\mu_z\rangle = 0.4\mu_B$, in line with high-field magnetization studies [17]. On the contrary, the estimated easy-axis direction corresponds to the crystallographic a axis and not the c axis, as previously reported in the neutron diffraction study of Ref. [14]. This apparent disagreement could evidence the presence of anisotropic two-ion magnetic exchange in $CeCuAl_3$ [18]. The value of $M^{\gamma,2}$ estimated from our analysis of the INS data is also in good agreement with perturbative calculations yielding $M^{\gamma,2} = 0.4$ meV/Ce^{3+} [19].

In summary, we have carried out INS measurements on the tetragonal $CeCuAl_3$ compound and found the presence of three magnetic excitations in the paramagnetic regime. These excitations cannot arise from pure CEF effects but rather originate from a vibron quasibound state, as also observed in the cubic compound $CeAl_2$. We used a vibron model with tetragonal point-group symmetry that satisfactorily explains the observed magnetic spectra for $CeCuAl_3$. We have calculated the vibron form factor and find it to be surprisingly similar to that corresponding to the $4f^1$ Ce^{3+} ion [19]. Such a vibron form factor agrees very well with the observed Q-dependent intensities of all three spectral features centered at 1.3, 9.8, and 20.5 meV. In this context, we have also investigated the magnetic INS excitations of $RCuAl_3$ compounds (R = Pr and Nd) and found that all observed CEF excitations can be explained on the basis of the pure CEF model [20]. It should be noted that despite the presence of strong MEL interactions, pressure studies up to 80 kbar do not show SC down to 2 K in $CeCuAl_3$ [21], a result which is to be contrasted with the emergence of pressure-induced SC in the NCS compounds $CeRhSi_3$ and $CeIrSi_3$ [10,11]. This observation may suggest that asymmetric spin-orbit coupling is more important than MEL coupling for this family of compounds in the SC state. All in all, the present INS study of the CEF-phonon-coupled $CeCuAl_3$ system highlights the increasing importance of detailed studies of the interplay between the magnetic and vibrational dynamics of strongly correlated electron systems in condensed matter physics.

We acknowledge interesting discussions with Profs B. D. Rainford, K. McEwen, A. Boothroyd, D. Paul, M. Loewenhaupt, and Dr. V. K. Anand and Dr. P. Manuel. We would like to thank to Dr. C. Stock for assistance during the MARI experiment, and Dr. W. Kockelmann and Dr. A. Daoud-Aladine for their help with the neutron diffraction measurements. We are grateful to the CMPC-STFC for providing research grant no. CMPC-09108 and Spanish and EU-Feder grant No. MAT2009-10040

*Corresponding author.
Devashibhai.adroja@stfc.ac.uk
†Also at Department of Physics and Astronomy, University College London, Gower Street, London, WC1E 6BT, United Kingdom.
‡Also at Materials Science Division, Argonne National Laboratory, Argonne, IL 60439-4845, USA.

[1] S. Chi *et al.*, Phys. Rev. Lett. **101**, 217002 (2008); E. A. Goremychkin and R. Osborn, Phys. Rev. B **47**, 14 280 (1993); A. D. Hillier, D. T. Adroja, P. Manuel, V. K.

Anand, J. W. Taylor, K. A. McEwen, B. D. Rainford, and M. M. Koza, Phys. Rev. B **85**, 134405 (2012).
[2] M. Loewenhaupt, B. D. Rainford, and F. Steglich, Phys. Rev. Lett. **42**, 1709 (1979).
[3] M. Loewenhaupt and U. Witte, J. Phys. Condens. Matter **15**, S519 (2003).
[4] P. Thalmeier and P. Fulde, Phys. Rev. Lett. **49**, 1588 (1982); P. Thalmeier, J. Phys. C **17**, 4153 (1984).
[5] C.-K. Loong, M. Loewenhaupt, J. C. Nipko, M. Braden, and L. A. Boatner, Phys. Rev. B **60**, R12549 (1999).
[6] L. C. Chapon, E. A. Goremychkin, R. Osborn, B. D. Rainford, and S. Short, Physica (Amsterdam) **378–380B**, 819 (2006).
[7] E. Mühle, E. A. Goremychkin, and I. Natkaniec, J. Magn. Magn. Mater. **72–78**, 81 (1989).
[8] C. H. Webster, L. M. Helme, A. T. Boothroyd, D. F. McMorrow, S. B. Wilkins, C. Detlefs, B. Detlefs, R. I. Bewley, and M. J. McKelvy, Phys. Rev. B **76**, 134419 (2007); J. Jensen, Phys. Rev. B **76**, 144428 (2007).
[9] O. Moze and K. H. J. Buschow, J. Alloys Compd. **245**, 112 (1996).
[10] N. Kimura, K. Ito, K. Saitoh, Y. Umeda, H. Aoki, and T. Terashima, Phys. Rev. Lett. **95**, 247004 (2005).
[11] H. Mukuda, T. Fujii, T. Ohara, A. Harada, M. Yashima, Y. Kitaoka, Y. Okuda, R. Settai, and Y. Onuki, Phys. Rev. Lett. **100**, 107003 (2008).
[12] E. Bauer, N. Pillmayr, E. Gratz, G. Hilscher, D. Gignoux and D. Schmitt, Z. Phys. **67**, 205 (1987); D. Werner, E. Bauer, J. M. Martin, M. R. Lees, Physica (Amsterdam) **259–261B**, 10 (1999).
[13] M. Kontani, H. Ido, H. Ando, T. Nishioka, and Y. Yamaguchi, J. Phys. Soc. Jpn. **63**, 1652 (1994).
[14] Y. Ohara, G. Motoyama, T. Nishioka, and M. Kontani, Technical Report of ISSP, Ser. A No. 3526, 1999.
[15] K. W. H. Stevens, Proc. Phys. Soc. London Sect. A **65**, 209 (1952); Rep. Prog. Phys. **30**, 189 (1967); Phys. Rep. **24**, 1 (1976).
[16] A. del Moral, *Handbook of Magnetostriction and Magnetostrictive Materials* (Del Moral Pub, Spain 2008), Vol. 2.
[17] G. Motoyama, K. Murase and M. Kontani, Jpn. J. Appl. Phys. Series **11**, 257 (1999).
[18] J. Jensen and A. R. Mackintosh, in *Rare Earth Magnetism* (Oxford Science Publications, Clarendon Press, Oxford 1991).
[19] A. del Moral (to be published).
[20] D. T. Adroja and V. K. Anand (to be published).
[21] Y. Kawamura, T. Nishioka, H. Kato, M.Matsumura, K. Matsubayashi, and Y. Uwatoko, J. Phys. Conf. Ser. **200**, 012082 (2010).